

Seoul National University Bright Quasar Survey in Optical (SNUQSO) I: First Phase Observations and Results

Induk Lee^{1,6}, Myungshin Im^{1,7}, Minjin Kim¹, Eugene Kang¹, Hyunjin Shim¹, Gordon T. Richards², Alastair C. Edge³, Myung Gyoong Lee¹, Changbom Park⁴, and Myeong-Gu Park⁵

ABSTRACT

We present results from the first phase of the Seoul National University Bright Quasar Survey in Optical (SNUQSO) as well as its basic observational setup. Previous and current large area surveys have been successful in identifying many quasars, but they could have missed bright quasars due to their survey design. In order to help complete the census of bright quasars, we have performed spectroscopic observations of new bright quasar candidates selected from various methods based on optical colors, near-infrared colors, radio, and X-ray data. In 2005/2006, we observed 55 bright quasar candidates using the Bohyunsan Optical Echelle Spectrograph (BOES) on the 1.8 m telescope at the Bohyunsan Optical Astronomy Observatory in Korea. We identify 14 quasars/Seyferts from our observation, including an optically bright quasar with $i = 14.98$ mag at $z = 0.092$ (SDSS J003236.59-091026.2). Non-quasar/Seyfert objects are found to be mostly stars, among which there are 5 M-type stars and one cataclysmic variable. Our result shows that there still exist bright quasars to be discovered. However, at the same time, we conclude that finding new bright quasars in high Galactic latitude regions is very challenging and that the existing compilation of bright quasars is nearly complete in the northern hemisphere.

Subject headings: galaxies: active - galaxies: nuclei - techniques: spectroscopic - quasars: individual (SNUQSO J003236.59-091026.2) - quasars: emission lines - surveys

¹Department of Physics and Astronomy, FPRD, Seoul National University, Seoul 151-747, Korea

²Department of Physics, Drexel University, 3141 Chestnut Street Philadelphia, PA 19104

³Institute for Computational Cosmology, Durham University, South Road, Durham DH1 3LE, UK

⁴Korea Institute for Advanced Study, Dongdaemun-gu, Seoul 130-722, Korea

⁵Kyungpook National University, Daegu 702-701, Korea

⁶idlee@astro.snu.ac.kr

⁷mim@astro.snu.ac.kr

1. Introduction

Since the first discovery of a quasar more than 40 yr ago (Schmidt 1963), many quasar surveys have been conducted to date, and the number of known quasars and Seyferts is now well over 100,000 (Véron-Cetty & Véron 2006; Croom et al. 2004; Schneider et al. 2007). Among numerous quasars discovered to date, bright quasars receive special attention as an attractive astrophysical tool. Since they are bright, one can investigate their intrinsic properties — such as the black hole mass and accretion rate — in detail, through long-term monitoring programs with small telescopes or getting high-resolution spectra (e.g., Kaspi et al. 2000; Hawkins 2007). By identifying more bright quasars, we can also possibly constrain the low-redshift luminosity function of quasars better, which can be useful for understanding the cosmological evolution of luminous quasars at high redshift.

There are many different techniques to find quasars, including UV-excess (UVX) method (Palomar-Green survey; PG), emission-line surveys using objective prisms (Hamburg Quasar Survey; HQS hereafter; Hagen et al. 1995), radio surveys (FIRST), and X-ray surveys. Here we describe a few major surveys related to bright quasars.

Optical surveys target point-like sources with UV excess (UVX) as quasar candidates. Quasars have a power-law spectrum, and the spectrum peaks at UV, which is called the UV bump. These unique spectral features distinguish quasars from normal stars. A representative large-area, bright quasar survey is the Palomar Bright Quasar Survey (BQS). BQS targeted 1715 UVX stellar objects with $U - B < -0.44$ mag and $B < 16.6$ mag chosen from a 10,714 deg² area of the northern sky covered by the Palomar Green Survey (PG; Schmidt & Green 1983). Among these 1715 objects, 92 (5.36%) were identified as quasars (Greene et al. 1986). More recently, large area galaxy surveys such as the Sloan Digital Sky Survey (SDSS) and the 2dF and 6dF surveys (Croom et al. 2004; Schneider et al. 2007) have discovered many quasars by selecting candidates mainly using multi-color selection criteria (Richards et al. 2002, 2004 ; Smith et al. 2005). The SDSS has improved optical quasar selection techniques by adopting sophisticated multi-color selection criteria (Richards et al. 2002, 2004). Richards et al. (2004) show that their quasar selection technique efficiency is more than $\sim 65\%$. Covering nearly the entire northern hemisphere, SDSS has found more than 70,000 quasars so far (Adelman-McCarthy et al. 2005).

Some other large-area bright quasar surveys—the Hamburg Quasar Survey (HQS, Hagen et al. 1995) and the Hamburg/ESO Survey (HES)—use objective prisms to identify emission line objects. HQS aims to cover $\approx 11,000$ deg² of the northern sky with digitized objective prism plates. HES plans to cover a similar area (9000 deg²) of the southern hemisphere with a similar technique. Both surveys target bright objects ($13 < B < 18$ mag for the northern hemisphere), and the HQS has found 343 bright quasars so far, 137 at $B \leq 17$ mag (Hagen

et al.1999). Fainter quasars are also discovered by other slitless spectroscopic surveys (e.g., Large Bright Quasar Survey by Hewett et al. 2001).

Bright quasars are also found by matching radio detections with optical point sources. As the name “quasar” stands for a radio source with stellar-like appearance, point sources with radio emission have a high probability of being a quasar. One of the largest radio-selected, bright quasar surveys is the FIRST Bright Quasar Survey (FBQS), which selects radio sources with compact optical appearance as quasar candidates. FBQS reports the discovery of 957 such objects (White et al. 2000 ; Becker et al. 2001).

These surveys cover significant portions of the sky, but it is quite possible that these surveys do not provide a complete census of bright quasars. Although SDSS has discovered nearly 100,000 quasars with its efficient survey strategy (Schneider et al. 2007), SDSS cannot discover very bright quasars because of technical difficulties related to the survey design. When spectroscopically observing targets selected from photometric data, SDSS imposes a magnitude limit at $i = 15.0$ mag, since the light from objects brighter than $i < 15$ mag spills over to neighboring fibers and ruins spectra of other targets. This leaves BQS, HQS, and FBQS as major sources of very bright quasars, but these surveys may have their own problems. Many works have been carried out to see if there are any systematic biases in BQS (Wampler & Ponz 1985; Goldschmidt et al. 1999; Miller et al. 1993). Such studies find that the photometric inaccuracy in BQS leads to omission of some bright quasars in their sample. For example, a recent work by Jester et al. (2005) shows that the photometric inaccuracy of the scanned photographic plate data used by BQS moves the actual $U - B$ cut to $U - B < -0.71$ from $U - B < -0.46$ as originally designed. Coupled with a photometric uncertainty of $\sigma_{U-B} = 0.24$ mag in the plate color, BQS seems to miss as many as 50% of bright quasars satisfying the magnitude cut. Although shown to be fairly complete (Wisotzki et al. 2000), an extensive search for bright QSOs might reveal QSOs missing from prism surveys. Radio surveys seem to be an effective way to find bright quasars, as White et al. (2000) show that most of bright quasars ($B < 16$) are also in the FIRST radio sources (Gregg et al. 1996; Becker et al. 2001). However, there might be bright quasars that are too radio-quiet to satisfy the FIRST detection.

In order to build more complete census of bright quasars ($i \lesssim 15$ mag), we have begun a bright quasar survey in the optical, called the Seoul National University Bright Quasar Survey in Optical (SNUQSO). Our survey plan is to use various quasar survey techniques (optical multi-color, near-infrared photometry, radio/X-ray) to search for any missing bright quasars from existing extensive quasar surveys. Our main scientific goals are (1) to discover any peculiar bright quasars; (2) to build complete census on bright quasars; and (3) to conduct follow-up observations of bright quasars to study host galaxy and SMBH properties

through long-term monitoring observations and high-resolution imaging.

In this paper, we report results from the first phase of this survey, which consists of the observations of bright quasar candidates at high Galactic latitude, selected from the public SDSS DR3 and DR4 releases, as well as NIR, radio, and X-ray data. Our results include the discovery of a very bright quasar and 13 other quasars/Seyferts. The second phase of the survey concentrates on quasars at low Galactic latitude, and it is currently ongoing. We will first describe the candidate selection method (section 2), followed by the observation and the data reduction procedure (section 3). In section 4, we will show the efficiency of the candidate selection method used in this study and describe the properties of the newly discovered quasar. Finally in section 5, we will summarize our findings and provide future plans. Note that we use throughout the paper the 2MASS photometric system for NIR data, and the AB magnitude system for SDSS magnitudes (see e.g., Fukugita et al. 1996). The current best-estimate of cosmological parameters of $H_0 = 71 \text{ km sec}^{-1}$, $\Omega_m = 0.27$, and $\Omega_\Lambda = 0.73$ (Spergel et al. 2003) is adopted when calculating the rest-frame quantities.

2. Sample Selection

This section describes various selection methods we used. We selected quasar candidates from three different data sets. The main data sets we used for our candidate selection are the SDSS Data Release 3 and 4 (hereafter DR3 and DR4, respectively) photometric data, *ROSAT* Bright Source Catalog (1RXS-B), NRAO VLA Sky Survey (NVSS; Condon et al. 1998) and Two Micron All Sky Survey (2MASS) Point Source Catalog (PSC). Also, we selected additional candidates from the Quasars.Org (QORG) catalog by Flesch & Hardcastle (2004) in order to test the QORG quasar selection method, which is also described later in this section. Table 1 summarizes targets observed so far. Note that the photometric data, presented in Table 1 is not corrected for Galactic extinction. Galactic extinction is small [$E(B - V) < 0.1 \text{ mag}$] for objects in Table 1 and does not affect our results nor selection of targets much.

2.1. Optical Multiple Color Method

As mentioned in §1, special characteristics of quasar SEDs place the majority of quasars in regions of color-color space away from stellar locus (e.g., Richards et al. 2002). The simplest example of the quasar selection based on color is the BQS UVX selection criterion of $U - B < -0.46 \text{ mag}$.

More sophisticated methods have been applied to the SDSS quasar selection (Richards et al. 2004; Schneider et al. 2007). Richards et al. (2002) isolate stellar locus in $ugriz$ multi-color space and select stellar objects outside the stellar locus as quasar candidates. Figure 14 in Richards et al. (2002) shows the location of quasars and stars in color-color spaces and how quasars can be effectively selected from such diagrams. More recently, Richards et al. (2004) have improved the quasar candidate selection using the “kernel density method”. We used this kernel density method on the SDSS DR3 data set to select bright quasar candidates. Note that these quasar candidates were picked as candidates in SDSS originally but not observed spectroscopically because they are too bright ($i < 15$ mag). With this method, we identified 44 bright quasar candidates, of which 22 were observable in 2005 January. We call these candidates group A candidates.

To find more bright quasars that might be missing in the kernel density method, we have gone back to a more straightforward color selection approach as well and selected additional candidates from the following color region:

$$\begin{aligned} 0.0 < u^* - g^* < 0.7, \\ -1.0 < g^* - r^* < 4.0, \\ -0.1 < r^* - i^* < 0.6, \\ \text{and } -0.3 < i^* - z^* < 0.5. \end{aligned}$$

The asterisk (*) denotes PSF magnitude, which is a magnitude measured by a PSF fitting method (Stoughton et al. 2002). The PSF magnitude should represent the total flux of a point source well. The above color box represents the region where many quasars can be found in color-color plots of Figure 7 in Richards et al. (2002). However, the above color box includes objects such as white dwarfs (WDs), M stars, or WD+M pairs. To improve the selection efficiency, we excluded the regions of WDs and WD+M pairs as defined in Richards et al. (2002).

First, the exclusion region of WDs is,

$$\begin{aligned} -0.8 < u^* - g^* < 0.7, \\ -0.8 < g^* - r^* < -0.1, \\ -0.6 < r^* - i^* < -0.1, \\ \text{and } -1.0 < i^* - z^* < -0.1, \end{aligned}$$

and the exclusion region of WD+M pairs is

$$-0.3 < g^* - r^* < 1.25,$$

$$0.6 < r^* - i^* < 2.0,$$

and $0.4 < i^* - z^* < 1.2.$

The SDSS photometry becomes inaccurate due to saturation for very bright point sources ($i < 14$ mag). Also, as we go to the brighter magnitude, the ratio of bright stars versus quasars satisfying the color selection criteria increases dramatically. As a consequence, the probability of a candidate being a quasar drops rapidly toward the brighter magnitude. Hence, we discarded candidates brighter than $i = 14$ mag. Through these processes, we selected about a hundred additional candidates for observation in 2005 January. We name these additional candidates group B candidates. Figure 1 shows the color boxes of group B candidates, WD, WD+M pairs, and the stellar locus. Note that the photometric data used in Figure 1 is not corrected for Galactic extinction as in Table 1.

2.2. Optical and Near IR

A number of studies suggest that quasars tend to have red colors in NIR, e.g., $J - K \gtrsim 2$ mag, while most stars have $J - K < 0.8$ mag (Cutri et al. 2000; Barkhouse & Hall 2001; Glikman et al. 2006; Maddox & Hewett 2006; Chiu et al. 2007). These studies imply that NIR data can be used to help identify quasars among point sources.

Therefore, we used NIR along with the optical selection to boost the selection efficiency of quasars during the 2005 May observation run. For this purpose, we expanded the faint limit of the magnitude cut to $i = 16$ mag, although this overlaps with the SDSS quasar observation. The $15 < i < 16$ candidates were not observed by SDSS spectroscopically at the time of our observation and served as a sample to test our optical + NIR color selection method. The optical + NIR color selection of quasar candidates was done via the following steps. First, we chose candidates using the optical multi-color method described in the previous section. In this case, we extended the color region a little to find more quasars. Then, we matched the selected objects with 2MASS point sources with $J - K > 0.8$ mag within $1''$ matching radius. This process yielded roughly 50 candidates, of which we observed 17. When observing these candidates, we have given more weights to objects with large $J - K$ values.

2.3. Radio + NIR Selection

It is well known that a point source with radio emission is likely to be a quasar (e.g., Becker et al. 2001; Hewett et al. 2001). By combining both the radio information and NIR color selection method, we can possibly discover quasars with minimal contamination from stars and other Galactic objects. To achieve this goal, we matched NRAO VLA Sky Survey (NVSS; Condon et al. 1998) radio sources against 2MASS objects with $J - K \gtrsim 1.4$ mag to select quasar/AGN candidates. Our test of the efficiency of such a method on SDSS quasars show a high quasar/Seyfert identification efficiency of $\gtrsim 85\%$. We observed five such quasar candidates at high Galactic latitude. They were observed in 2006 June/December runs together with 88 low Galactic latitude quasar/AGN candidates as reported in Im et al. (2007). The detailed description of the sample selection appears in Im et al. (2007) and I. Lee et al. (2008, in preparation).

2.4. X-ray Sources

It has been known that many quasars are X-ray sources (e.g., Stocke et al. 1991). This means that X-ray selection can help select quasars. To select quasar candidates, we used the *ROSAT* All-Sky Bright Source Catalog (1RXS-B), for which the positional accuracy is known to be $\sim 13''$ (68% confidence; Voges et al. 1999). We matched X-ray sources in 1RXS-B against 2MASS point sources with $J - K > 1$ mag and $J < 16$ mag within the matching radius of $10''$ and chose them as quasar candidates. Therefore, this selection method is based on X-ray + NIR data.

2.5. QORG catalog

As additional targets, we chose objects having a high probability of being quasars in the QORG catalog of Flesch & Hardcastle (2004). Flesch & Hardcastle matched radio and/or X-ray sources to optical sources in the APM/USNO-A catalogs. Then, they assigned a possible optical match to the X-ray/radio detections based on the probability that the optical match is a quasar. The probability is based on the color, the appearance (extended vs. point), and the local density of optical sources around the X-ray/radio detection. We observed six targets from the QORG catalog as filler targets.

3. Observation and Data Reduction

3.1. Observation

We observed quasar candidates with the longslit, low resolution mode of Bohyunsan Optical Echell Spectrograph (LSS; Kim et al. 2003) on the 1.8 m telescope at the Bohyunsan Optical Astronomy Observatory (BOAO), Korea, over four observing runs spanning from 2005 January to 2006 December. Table 2 summarizes the weather conditions and observing parameters of each run.

For our spectroscopic observation, we used a 150 groove mm^{-1} grating and a slit with a width of 250 μm . The width and the length of the slit correspond to 3.6'' and 3.6' on the sky, respectively. This spectroscopic setup provides a wide wavelength coverage of $\Delta\lambda \simeq 5000 \text{ \AA}$, and 5.2 $\text{\AA}/\text{pixel}$ with a resolution of $\lambda/\Delta\lambda \sim 366$ or $\delta v \sim 820 \text{ km sec}^{-1}$ in full width at half-maximum (FWHM). The instrument spectral resolution has been measured from the comparison lamp spectra. In order to cover as much wavelength as possible for identifying multiple lines for redshift identification, we have chosen to use rather low-resolution but wide-wavelength coverage as the spectroscopic setup. With our spectroscopic setup, we can detect $H\alpha$ (6563 \AA) from $z = 0$ to $z = 0.5$, $H\beta$ (4861 \AA) from $z = 0.028$ to $z = 1.0$, [O III] 5007 \AA from $z = 0$ to $z = 0.99$, and [O II] 3727 \AA doublet from $z = 0.342$ to $z = 1.683$. For high-redshift objects, Mg II (2798 \AA , $z = 0.787$ to 2.574) and C IV (1549 \AA , $z = 2.228$ to 5.456) are useful redshift indicators. The slit width matches the poor seeing condition of the BOAO site. The spectrum is dispersed on a 1024-by-1024 CCD, whose spatial plate scale is 0.73'' pixel^{-1} . A detailed description of BOES-LSS system in BOAO is given in Kim et al. (2003).

The weather during the observing runs was not very good, but we managed to observe 55 candidates in total. Typically, exposures were taken twice for each candidate, with about 5-10 minutes for each exposure depending on the brightness of the target and the sky condition. We shifted the position of the target on the slit by about 1' before taking the second exposure for each candidate. When there was another point source near the candidate, if it had a similar color to the candidate, we tried to observe it also. The spectra of the comparison lamp, FeNeArHe, were taken right before and after each exposure for the wavelength calibration. We also observed several spectrophotometric standard stars for flux calibration. We used tungsten halogen lamps (THL) for a flat field.

3.2. Reduction

We reduced all the data using IRAF¹ packages. The data were reduced with the standard procedures of bias subtraction, flat-fielding, aperture extraction, wavelength calibration, and flux calibration.

Since the seeing condition was not stable each night and some of the nights were non photometric, the above flux calibration includes some inaccuracies. To improve the flux calibration, we renormalized the spectrum for a newly discovered quasar (see next section). This renormalization is done by adjusting the flux-calibrated spectrum to match the known photometric information of the object. For this purpose, we used the SDSS photometric data. Comparison of the SDSS photometry and the spectrum with the original flux calibration reveals that the flux of the spectrum is underestimated compared to the SDSS photometry by 8.1%, 19.8%, and 25.0% in the g , r , and i bands, respectively. To reduce the difference, we recalibrated the flux of the spectrum to match the SDSS photometry at r band. This comparison shows that the flux calibration is accurate for the renormalized quasar spectrum at about the 10% level. We have not performed renormalization of the flux calibration for the other objects, but the above exercise suggests that the flux value is accurate to about 25%.

Finally, we measured the redshift by running the ‘xcsao’ task of ‘rvsao’ package. The observed wavelengths of the $H\alpha$, $H\beta$, and [OIII] are matched with the emission line templates, and the recession velocity of each object is determined by a cross-correlation technique.

4. RESULTS

We observed 17, 17, 5, 10, and 6 quasar candidates from the optical multi-color selected sample (section 2.1), the optical+NIR color selected sample (section 2.2), the radio+NIR color selected sample (section 2.3), the X-ray+NIR color selected sample (section 2.4), and the QORG sample (section 2.5), respectively. Among these objects, we confirmed that 1, 3, 4, 6, and 0 are quasars. Spectroscopic properties of these 14 quasars/Seyferts are presented in Table 3. Some of them were also discovered by SDSS after our observation, and such cases are marked in Table 1 and 3.

¹“IRAF is distributed by the National Optical Astronomy Observatory, which is operated by the Association of Universities for Research in Astronomy, Inc., under cooperative agreement with the National Science Foundation.”

4.1. Newly Discovered Quasars

Fig. 2 and Fig. 3 show the flux calibrated spectra and images of newly discovered quasars/Seyferts. The spectra in Fig. 2 show strong [OIII] emission lines or broad emission lines which are characteristic of quasars/Seyferts. Table 3 lists the parameters of each quasar such as redshifts, coordinates, FWHMs, and absolute magnitudes for the g and i bands. We classify objects as quasars when their Balmer line FWHM widths exceed 1000 km s^{-1} and their absolute magnitudes are brighter than $M_i = -22 \text{ AB mag}$ (Schneider et al. 2003). Three objects, J143008.65+230621.6, J153334.69+051311.4, and J160731.42+173138.4 in Table 3, are found to have $M_i > -22 \text{ AB mag}$, and therefore we classify these objects as Seyferts. One exception is the object J112632.90+120438.0, for which an emission line was marginally detected. This object was later identified as a broad-line quasar at $z = 0.977$ by SDSS. Therefore, we include this object in the list of quasars.

The line widths are measured for two emission lines, $H\alpha$ and $H\beta$, using a single-component Gaussian-fitting, instead of a two-component profile of narrow+broad lines (e.g., Kim et al. 2003), since the spectral resolution is not high enough to effectively separate the two components. Note that this procedure can underestimate the broad line width. The continuum of the spectrum under each emission line was determined by a straight line interpolation between two points that lie sufficiently far from the emission line. We tried several different sets of two points to see how the FWHM values change, but did not find any significant variation for $H\alpha$. The above procedure did not work as well for $H\beta$ since the $H\beta$ lies in a part of the spectrum where calibration is in suspect (see section 4.2). The instrument resolution was also corrected for the line width measurements.

When deriving the absolute magnitudes, we used a K -correction assuming a power law of $f_\nu \propto \nu^\alpha$, ignoring host galaxy and emission line contribution (see §5.4.). In such a case, K -correction can be expressed as a simple form of $K(z) = -2.5(\alpha + 1) \log(1 + z)$, and we used the value of $\alpha = -0.5$ (Schmidt & Green 1983; Boyle et al. 1988). Note that for objects where the host galaxy is clearly visible (J102700.00+390804.2, J103858.44+401058.4, J124127.66+085219.5, J143008.65+230621.6, J145434.35+080336.7, J153334.69+051311.4, and J160731.42+173138.4), the absolute magnitudes in Table 3 serve only as a rough measure, since we ignored the host galaxy light in calculating the absolute magnitudes. Also we estimate that the contribution of $H\alpha$ to the total flux in i band can be as much as $\sim 25\%$.

The most notable discovery is SNUQSO J003236.59-091026.2, which ranks among the brightest quasars discovered to date [$i = 14.98 \text{ mag}$ or $V=15.3 \text{ mag}$, adopting the relation of $V = g - 0.52(g - r) - 0.03$ in Jester et al. 2005]. To determine where this quasar ranks in terms of apparent brightness, we matched SNUQSO J003236.59-091026.2 against

a list of known quasars searched in the NASA/IPAC Extragalactic Database (NED)². A simple NED search reveals that this quasar corresponds to the 5th–14th brightest at V -band among bona fide “pointlike” quasars (as of 2007 July 16). In any case, the discovery of SNUQSO J003236.59-091026.2 suggests that there still exist very bright quasars waiting to be discovered, although the number of such objects might be very small.

4.2. Non-Quasars and Unidentified Objects

Fig. 4 shows the representative spectra of objects classified as stars, as well as interesting stellar objects such as M stars and a cataclysmic variable. We identified objects as stars if their spectra show $H\alpha$ absorption line at low radial velocity. Only one of the candidates (J105756.30+092314.9) other than quasar/AGNs showed a clear sign of an emission line at $H\alpha$. The velocity dispersion of this object is found to be $\sigma_v \simeq 375 \text{ km s}^{-1}$, and we classify this as a cataclysmic variable star from the spectral feature and the identification of $H\beta$ and $H\gamma$ lines using additional data we obtained in 2005 February. In addition, we identify five M stars based on their spectral shapes. However, except for J043737.4-022928A, they are located very close to another brighter star, and the spectra of these stars might be contaminated by nearby stars. For other stars, we could not classify spectral types, because of the limited spectral coverage we used at blue wavelengths (5000–10000Å or 4200–8400Å) and concerns about the calibration at 5000–6000Å where an artificial bump appears possibly due to instrument defects.

5. DISCUSSIONS

5.1. Quasar Selection Efficiency

Here we examine the quasar selection efficiency of various methods, which is summarized in Table 4.

5.1.1. Optical Multiple Color Method

For the optical multiple color method, we found only one quasar out of group A and B targets (17 total). Therefore, the efficiency of our candidate selection method seems very

²<http://nedwww.ipac.caltech.edu>

low, which is consistent with Richards et al. (2006), who find the efficiency of the optical multiple color (*ugri*) selection method at bright end ($i < 15.5$ mag) is less than 5%. To find ways to improve the bright quasar selection efficiency, we examine the property of targets in more detail.

The newly discovered quasar, SNUQSO J003236.59-091026.2, is detected in both radio and IR. Two objects selected with this method are found to be radio sources; therefore, the efficiency is 50% if the selection was done using radio detection. Although this number is based on small number statistics, it is interesting to note that the efficiency is consistent with that of FBQS (e.g. White et al. 2000).

In the case of nonradio, optically selected bright quasar candidates, none turned out to be quasars. Therefore, we conclude that it is very unlikely to find an optically selected bright quasar that is not a radio source. We can think of two reasons for this low efficiency. The first reason could be stellar contamination. The surface density of quasars decreases toward bright magnitudes, while the number of stars does not change much. Therefore, the optical selection tends to pick up more stars than quasars at bright magnitudes. Second, the majority of optically bright quasars are detectable in radio at the current radio survey limits. For example, Fig. 13 of White et al. (2000) shows that the surface density of radio-selected quasars is almost the same as that of optically selected quasars at bright magnitude, suggesting that the optical bright quasars have almost complete overlap with radio-selected quasars.

5.1.2. Other Methods

For the optical+NIR color selection method, we find that the efficiency is 17.6%. Three quasars identified with this method are found to have $J - K > 1.5$ mag and $15 < i < 16$. This re-confirms the idea that point sources with non-stellar optical colors and red, NIR colors are likely to be quasars.

For the radio+NIR color selection method, we find that the identification efficiency is quite high (80%). This is consistent with the value we obtain through simulations using SDSS quasars (I. Lee, et al. 2008, in preparation). This is not surprising, considering that this selection method is a combination of two efficient quasar identification methods

For the X-ray selected targets, we find the identification efficiency at its face value is about 60%. This confirms that X-ray data are quite valuable for finding AGNs, especially when the data are combined with NIR colors.

For QORG targets, we could not find any quasar or AGN. The quasar SNUQSO J003236.59-091026.2 could have been in the QORG catalog, but it appears that the quasar was mismatched to a star with $i = 13.8$ mag, $6''$ away from SNUQSO J003236.59-091026.2.

5.2. Radio Properties of New Quasars

Fig. 5 shows broadband SEDs of several new quasars from UV to radio wavelengths. In Fig. 5, we also plot SEDs of well-known radio-loud quasars. The figure indicates that the newly discovered quasars have lower fluxes at radio than typical radio-loud quasars. In order to measure the radio loudness, we calculated the radio loudness parameter R^* for each QSO. The R^* parameter is taken as the ratio of flux in radio at 6 cm versus optical flux at 4400 \AA , and for radio-loud quasars, the R^* value exceeds 10 (Kellermann et al. 1989; Stocke et al. 1992). When calculating R^* parameter, we adopt g -band flux as the flux at 4400 \AA and the 6 cm flux is computed from the 21 cm flux assuming a power law of $f_\nu \sim \nu^{-0.46}$ (Ho & Ulvestad 2001). When quasars do not appear in the NVSS catalog or in the FIRST catalog, we derived upper limits of R^* using the detection limit of the NVSS survey ($\approx 2.5 \text{ mJy}$).

The radio loudness of quasars is summarized in Table 3. We find that only one of them belongs marginally to the radio-loud category. Thus, we can conclude that the majority of the newly discovered QSOs are radio-quiet.

5.3. Mass of Black Holes

We estimate the mass of supermassive black hole residing in quasars using the method of Greene & Ho (2005) which uses $L_{H\alpha}$ and σ_v of $H\alpha$ with,

$$M_{BH} = 2.0^{+0.4}_{-0.3} \times 10^6 \left(\frac{L_{H\alpha}}{10^{42} \text{ erg s}^{-1}} \right)^{0.55 \pm 0.02} \left(\frac{\text{FWHM}_{H\alpha}}{10^3 \text{ km s}^{-1}} \right)^{2.06 \pm 0.06} M_\odot. \quad (1)$$

The estimated M_{BH} -values are presented in Table 3. We find that the SMBH masses range between 10^7 and $10^9 M_\odot$. For SNUQSO J003236.59-091026.2, it is about $2.6^{+0.9}_{-0.9} \times 10^7 M_\odot$.

5.4. Host Galaxies

In this section, we examine the properties of the host galaxies and their detectibility.

We use the σ_v and M_{BH} correlation of Tremaine et al. (2002) to get σ_v and then obtain the host spheroid luminosity L using the Faber-Jackson relation.

Table 5 lists the host galaxy σ_v and the luminosity. The host spheroid systems expect to have various mass properties in the range $\sigma_v = 60\text{--}350 \text{ km s}^{-1}$.

In order to check the detectibility of the host galaxies, we examined their expected apparent brightnesses and sizes. The apparent magnitudes are estimated by adopting the

K -correction of $K_{\text{corr},\text{gal}}(z) = z \text{ mag}$ for i band, and the rest-frame color of $B - i = 1.75 \text{ mag}$ and $B - g = 0.5 \text{ mag}$ of early-type galaxies (Fukugita et al. 1995). In order to estimate the apparent size, we calculate the r band half-light radius, \bar{r}_{50} from the $\bar{r}_{50} - M_v$ relation of McIntosh et al. (2005).

The derived properties of host galaxies are listed in Table 5. It is interesting to compare the predicted host galaxy luminosity versus the observed host galaxy brightness for quasars for which host galaxies are visible (J102700.00+390804.2, J103858.44+401058.4, J124127.66+085219.5, J143008.65+230621.6, J145434.35+080336.7, J153334.69+051311.4, J160731.42+173138.4 in Fig. 3). Assuming that the fiber magnitude (3'' diameter) represents the light from a bright, central region, we attempted to measure a rough value of the host galaxy luminosity by subtracting fiber magnitude from the Petrosian magnitude. The measured values mostly are brighter by up to a few magnitudes, or similar to the predicted host galaxy luminosities within a few tenths of a magnitude, which is not very surprising considering that the predicted host galaxy luminosities take into account the luminosity of spheroidal components only. One exception is J153334.69+051311.4, whose predicted magnitude is about 1 mag fainter than the Petrosian-Fiber magnitude. The Petrosian magnitude of this object is similar to the predicted i magnitude, therefore we suspect that the Fiber magnitude is not a good representation of the central point source in this case.

For the other cases, the host spheroids seem to be not only much fainter (by a few magnitudes) than the quasars but also small in their apparent sizes. Therefore, finding an underlying host galaxy would require a high-resolution imaging with high contrast, and the apparent absence of the host galaxy image in the SDSS imaging data seems natural.

6. Conclusion

We have carried out a bright quasar survey to discover new bright quasars that have been missed in previous surveys. Bright quasar candidates are selected from SDSS and 2MASS data in several ways, including the optical multi-color method, the optical+NIR

color selection method, the radio+NIR color selection method, and the X-ray+NIR color selection method. Some candidates are also taken from the QORG catalog. Our spectroscopic observations of 55 targets at the BOAO observatory reveal 14 new bright quasars, while most of the other targets are found to be stars including 1 cataclysmic variable and 5 M-types. Among 24 optically selected or optical+NIR color selected $i < 15$ mag quasar candidates, only SNUQSO J003236.59-091026.2 has been identified as a new quasar. There still exist very bright quasars missing in previous surveys, although the number of such “missed” bright quasars is probably very small. The use of multiwavelength data sets proves to be a more efficient way to find bright quasars. When applied to $i \lesssim 17$ mag candidates, these selection methods uncovered 13 quasars out of 25 candidates. Six candidates from the QORG catalog are found to be stars.

We have studied the properties of the new quasars as well. For SNUQSO J003236.59-091026.2, we estimate an SMBH mass of $2.6 \times 10^7 M_\odot$, suggesting that the host galaxy of this quasar is similar to a dwarf elliptical M32, the bulge of the Milky Way, or M32. The close proximity of this object to a neighbor star ($i = 13$ mag, $6''$ apart) makes SNUQSO J003236.59-091026.2 a good target for adaptive optics observation from the ground. The SMBH mass of other quasars ranges from 10^6 to $10^9 M_\odot$.

Despite our discovery, we find that the probability of finding very bright quasars ($i < 15$ mag) not in existing catalogs is very low, and the previous list seems almost complete for bright quasars at high Galactic latitude regions in the northern hemisphere.

This work was supported by grant R01-2005-000-10610-0 from the Basic Research Program of the Korea Science and Engineering Foundation. Also, I.L., M.K., E.K., and H.S. are supported in part by the Brain Korea 21 program at Seoul National University. C.B.P and M.G.P. acknowledge the support of the Korea Science and Engineering Foundation (KOSEF) through the Astrophysical Research Center for the Structure and Evolution of the Cosmos (ARCSEC). Funding for the SDSS and SDSS-II has been provided by the Alfred P. Sloan Foundation, the Participating Institutions, the National Science Foundation, the US Department of Energy, the National Aeronautics and Space Administration, the Japanese Monbukagakusho, the Max Planck Society, and the Higher Education Funding Council for England. The SDSS Web site is <http://www.sdss.org/>. The SDSS is managed by the Astrophysical Research Consortium for the Participating Institutions. The Participating Institutions are the American Museum of Natural History, Astrophysical Institute Potsdam, University of Basel, University of Cambridge, Case Western Reserve University, University of Chicago, Drexel University, Fermilab, the Institute for Advanced Study, the Japan Participation Group, Johns Hopkins University, the Joint Institute for Nuclear Astrophysics, the Kavli Institute for Particle Astrophysics and Cosmology, the Korean Scientist Group,

the Chinese Academy of Sciences (LAMOST), Los Alamos National Laboratory, the Max-Planck-Institute for Astronomy (MPIA), the Max-Planck-Institute for Astrophysics (MPA), New Mexico State University, Ohio State University, University of Pittsburgh, University of Portsmouth, Princeton University, the United States Naval Observatory, and the University of Washington. We thank Sangak Lee, Marcel Agueros, Don Hoard, and others for their useful inputs on stellar classification, and Yoojae Kim and Kyungsook Chung for obtaining the spectrum of the cataclysmic variable star discussed in the paper. Also, we thank the staffs at BOAO, especially Kang-Min Kim and Byeong-Cheol Lee for their professional aid during our observing run.

Facilities: BOAO 1.8m telescope, BOES LSS

REFERENCES

- Adelman-McCarthy, J., et al. 2006, *ApJS*, 162, 38
- Barkhouse, W. A., & Hall, P. B. 2001, *AJ*, 121, 2843
- Becker, R. H., et al. 2001, *ApJS*, 135, 227
- Boyle, B. J., Shanks, T., & Peterson, B. A. 1988, *MNRAS*, 235, 935
- Chiu, K., et al. 2007, *MNRAS*, 375, 1180
- Condon, J. J., et al. 1998, *AJ*, 115, 1693
- Croom, S. M., et al. 2004, *MNRAS*, 349, 1397
- Cutri, R. M., et al. 2000, in *The New Era of Wide-Field Astronomy*, ed. R. Clowes (San Francisco : ASP), 232
- Flesch, E., & Hardcastle, M. J. 2004, *A&A*, 427, 387
- Fukugita, M., Shimasaku, K., & Ichikawa, T. 1995, *PASP*, 107, 945
- Fukugita, M., et al. 1996, *AJ*, 111, 1748
- Glikman, E., Helfand, D. J., & White, R. L. 2006, *ApJS*, 640, 579
- Goldschmidt, P., et al. 1999, *ApJ*, 511, 612
- Greene, J. E., & Ho, L. C. 2005, *ApJ*, 630, 122

- Green, R. F., Schmidt, M., & Liebert, J. 1986, ApJS, 61, 305
- Gregg, M. D. et al. 1996, AJ, 112, 407
- Hagen, H.-J., Engels, D., & Reimers, D. 1999, A&AS, 134, 483
- Hagen, H.-J. et al. 1995, A&AS, 111, 195
- Hawkins, M. R. S. 2007, A&A, 462, 581
- Hewett, P. C., Foltz, C. B., & Chaffee, F. H. 2001, AJ, 122, 518
- Hewett, P. C., Foltz, C. B., & Chaffee, F. H. 1995, ApJ, 109, 149
- Ho, L. C., & Ulvestad, J. S. 2001, ApJS, 133, 77
- Im, M., et al. 2007, ApJ, 664, 64
- Jester, S., et al. 2005, AJ, 130, 873
- Kaspi, S., et al. 2000, ApJ, 533, 631
- Kellermann, K. I., et al. 1989, AJ, 98, 1195
- Kim, K.-M., et al. 2003, Publ. Korean Astron. Soc. , 18, 81
- Maddox, N., & Hewett, P. C. 2006, MNRAS, 367, 717
- McIntosh, D. H., et al. 2005, ApJ, 632, 191
- Miller, P., et al. 1993, MNRAS, 263, 425
- Richards, G. T., et al. 2002, AJ, 123, 2945
- Richards, G. T., et al. 2004, ApJS, 155, 257
- Richards, G. T., et al. 2006, AJ, 131, 2766
- Schmidt, M., 1963 Nature, 197, 1040S
- Schmidt, M., & Green, R. F. 1983, ApJ, 269, 352
- Schneider, D. P., et al. 2007, AJ, 134, 102
- Schneider, D. P., et al. 2003, AJ, 126, 2579
- Smith, R. J., et al. 2005, MNRAS, 359, 57

- Spergel, D. N., et al. 2003, ApJS, 148, 175
- Stocke, J. T., et al. 1991, ApJS, 76, 813
- Stocke, J. T., et al. 1992, ApJ, 396, 487
- Stoughton, C., et al. 2002, AJ, 123, 485
- Tremaine, S., et al. 2002, ApJ, 574, 740
- Véron-Cetty, M.-P., & Véron, P. 2006, A&A, 455, 773
- Voges, B. W., et al. 1999, A&A, 349, 389
- Wampler, E. J., & Ponz, D. 1985, ApJ, 298, 448
- Wisotzki, L., et al. 2000, A&A, 358, 77
- White, R. L., et al. 2000, ApJS, 126, 133

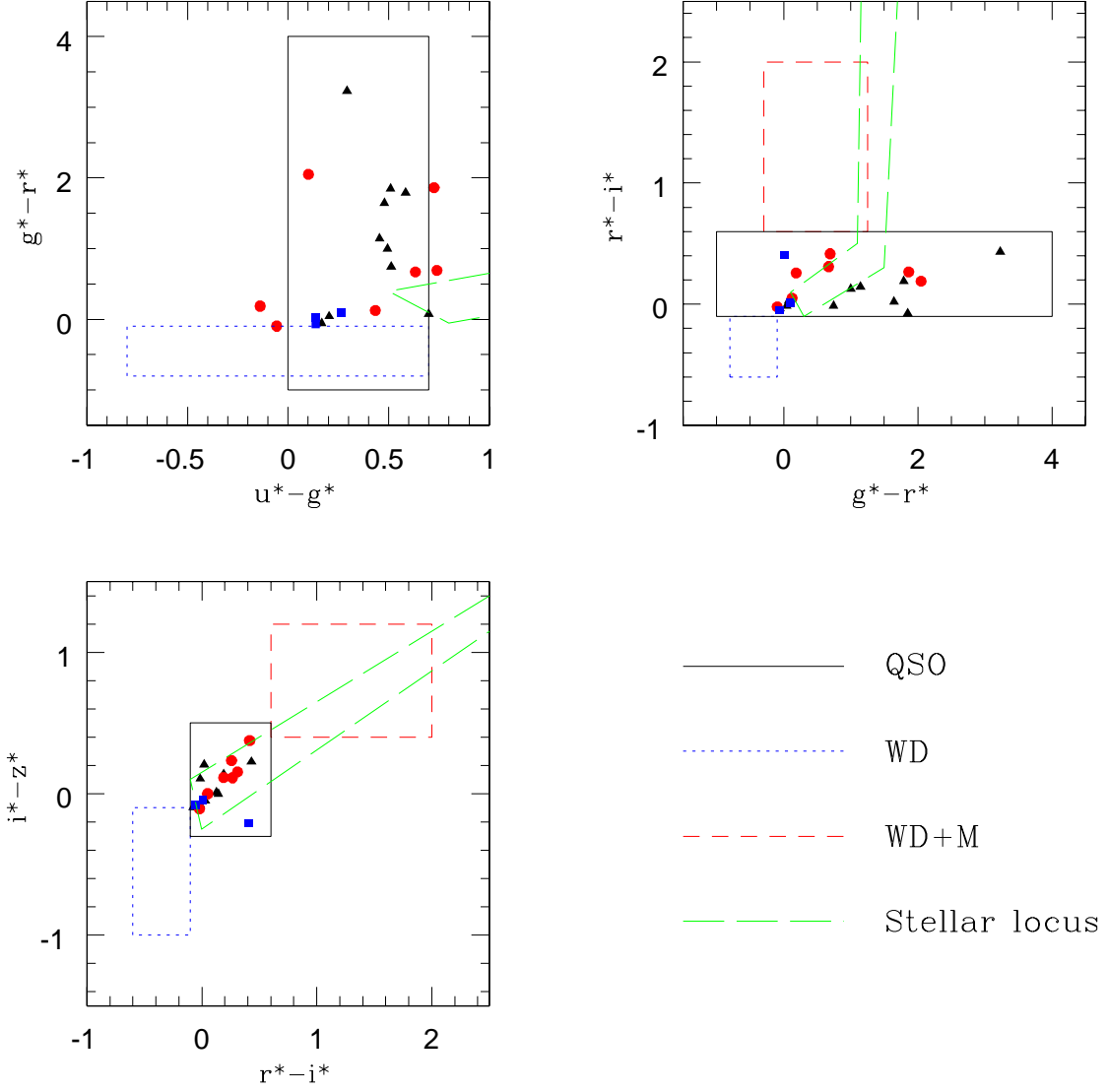


Fig. 1.— Color-color plot of observed targets. Red circles and blue triangles indicate group A and group B candidates, respectively, and squares show candidates that satisfy both group A and group B criteria. Black solid, blue dotted, and red short dashed boxes represent quasar, white dwarf, and white dwarf + M star regions, respectively. Green long dashed boundary shows location of the stellar locus.

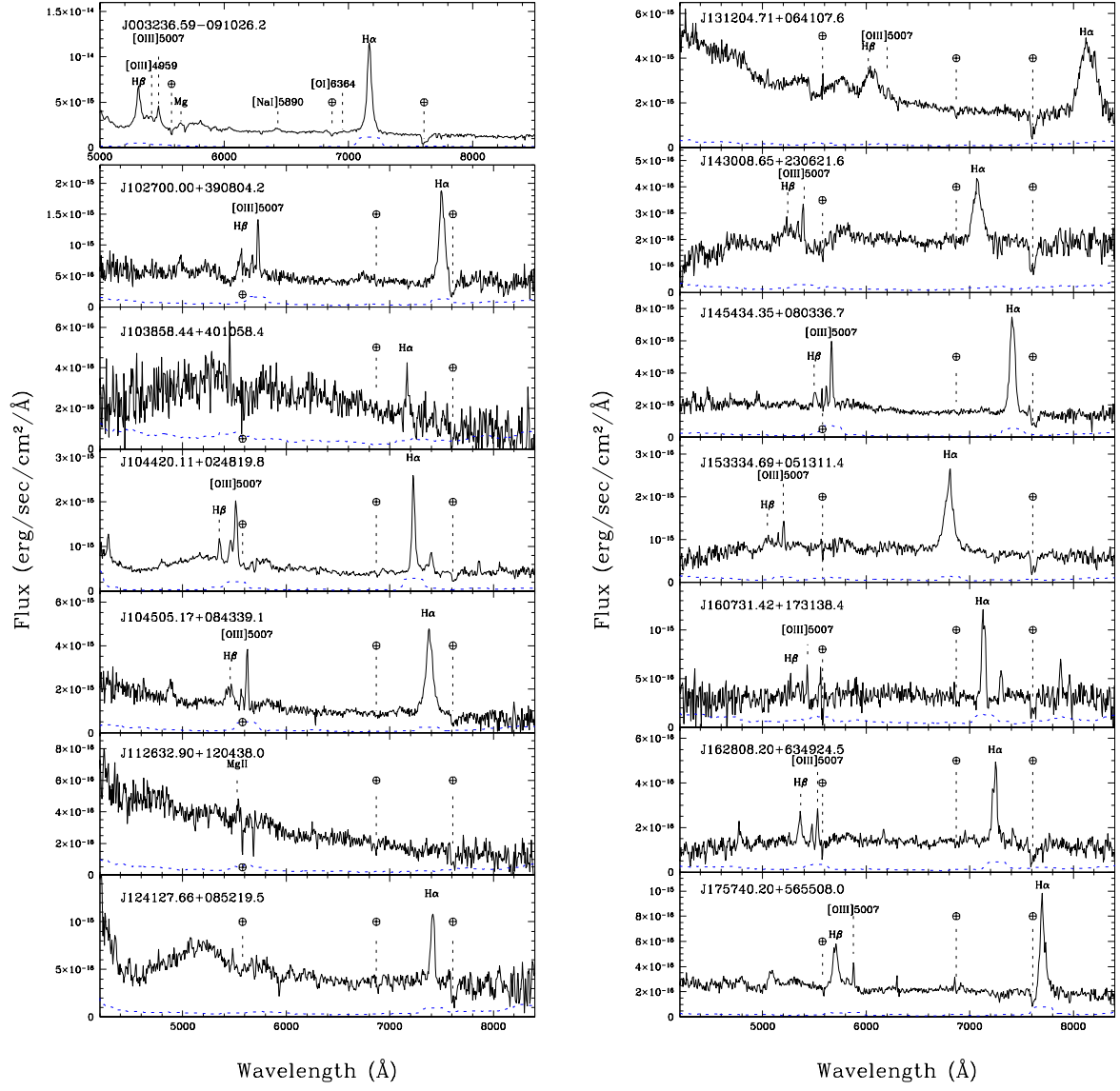


Fig. 2.— Spectra of newly discovered quasars. The dashed lines indicate 1 σ error. Symbol \oplus shows the positions of the sky absorption lines.

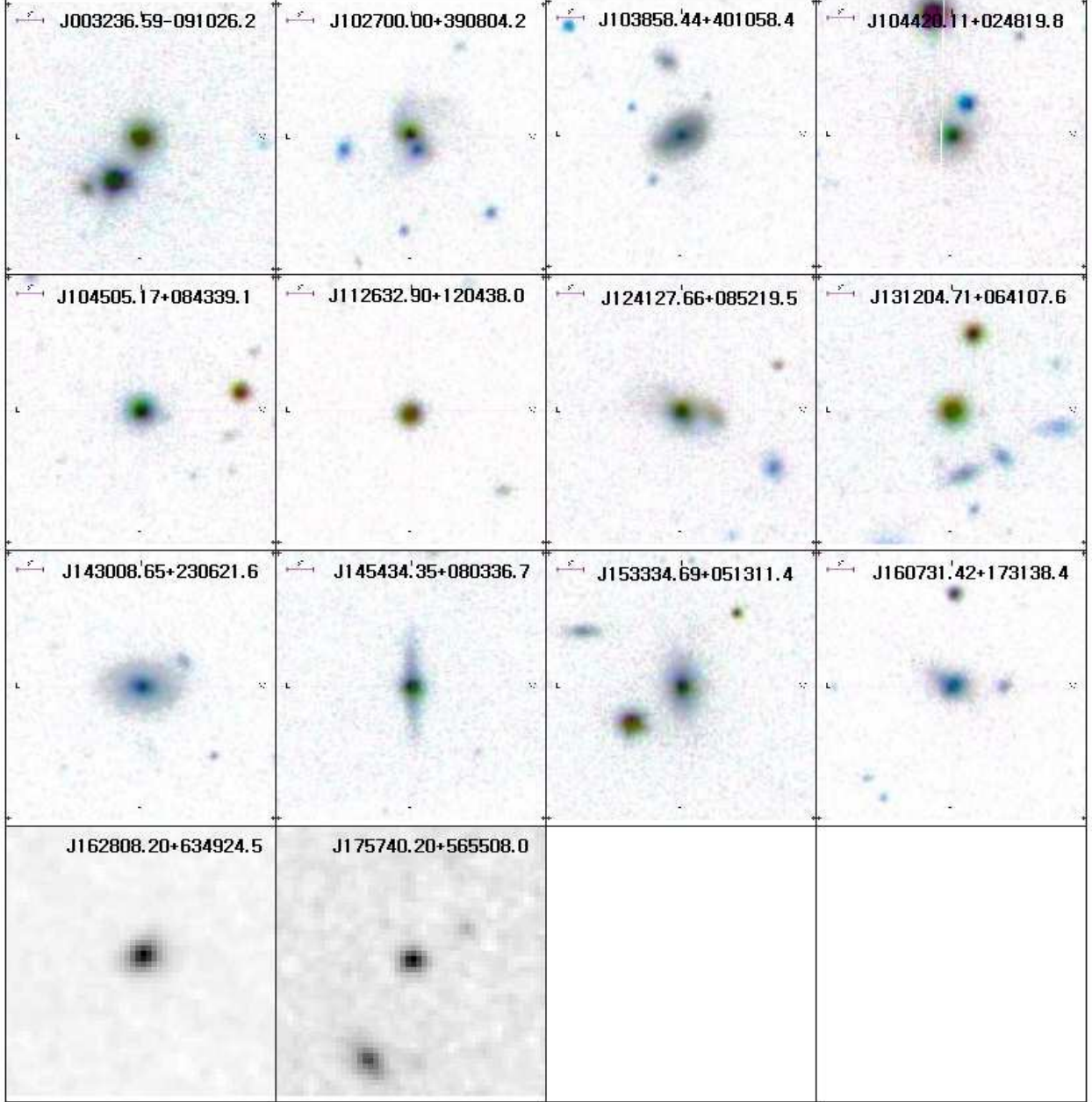


Fig. 3.— 50'' \times 50'' images of newly discovered quasars. The images of 'J003236.59-091026.2' through 'J153334.69+051311.4' are color-composites of *g* (blue), *r* (green), and *i* (red) images taken from the SDSS database. The images of 'J160731.42+173138.4' through 'J175740.20+565508.0' are from POSS-II red plate data.

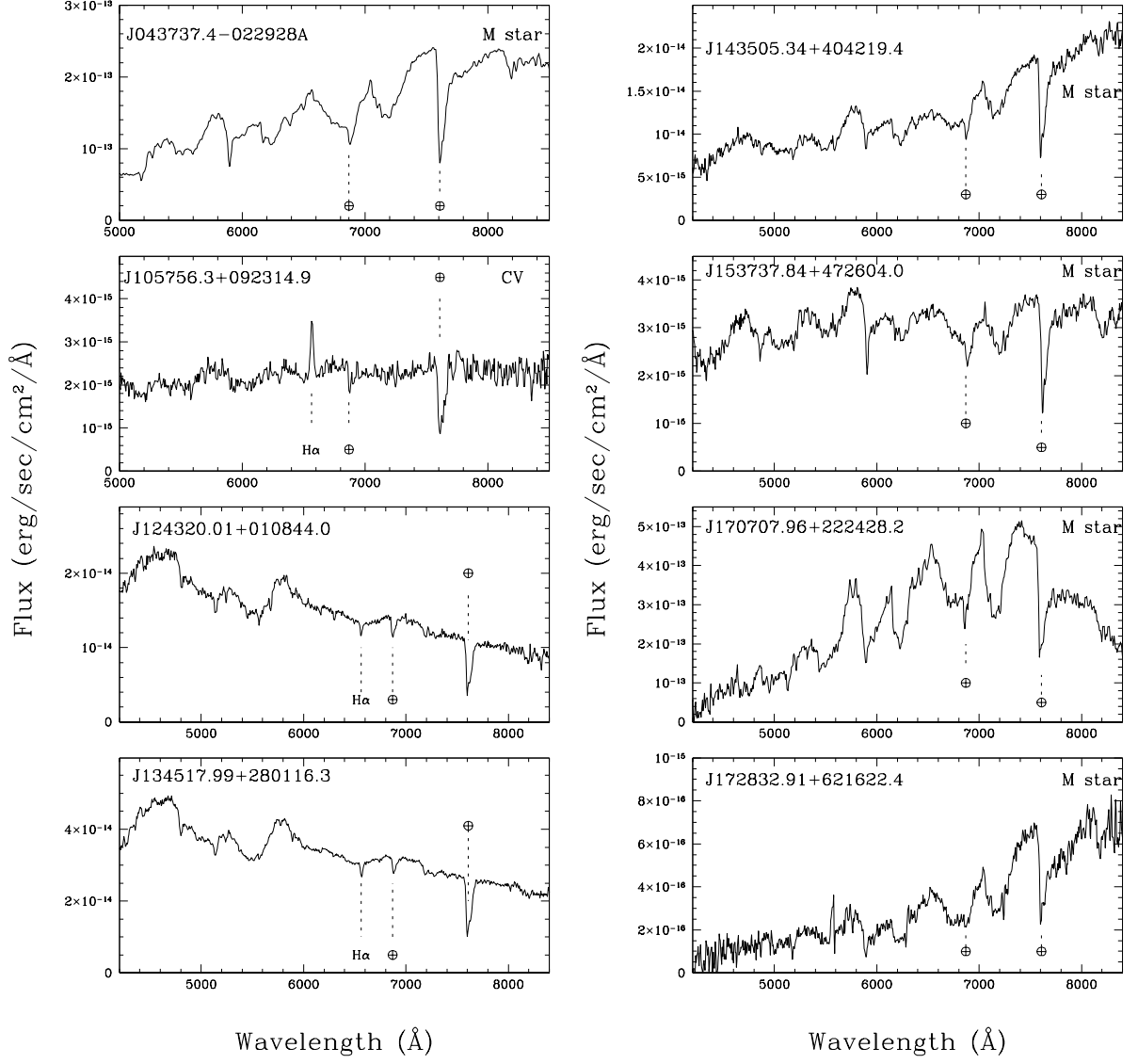


Fig. 4.— Representative spectra of several objects identified as stars, including a cataclysmic variable and M stars.

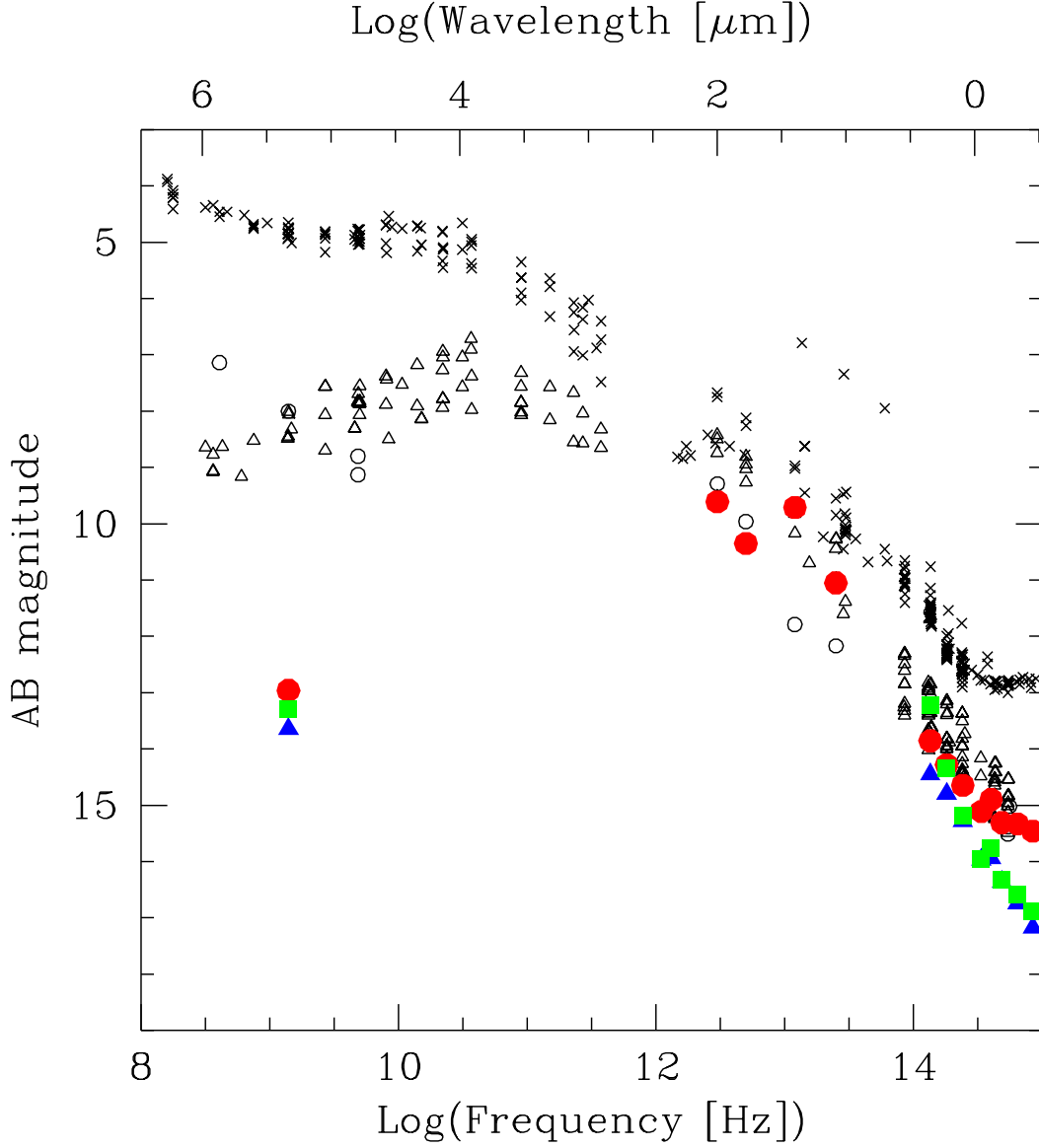


Fig. 5.— Spectral energy distributions of 6 quasars. Crosses are for 3C273, open triangles for OJ+287, open circles for 3C066A, red filled circles for SNUQSO J003236.59-091026.2, blue filled triangles for SNUQSO J145434.35+080336.7, and green filled squares are for SNUQSO J104505.17+084339.1. The data of 3 quasars, 3C 273, OJ+287, and 3C 66A, are taken from NED.

Table 1. Target summary

Name	Type ^a	Method	z^b	$J - K$	Group	SDSS? ^c
J000315.82+004017.8	Star	Optical	14.43	0.41	B	No
J001002.11+004809.6	Star	Optical	14.46	0.44	B	No
J003236.59–091026.2	Quasar	Optical	14.98	1.99	Both	Yes
J005229.4+001456	Star	QORG				No
J012055.4+000454	Star	QORG				No
J021505.57–091606.5	Star	Optical	14.09	0.24	B	Yes
J025058.8+001226	Unknown	QORG				No
J043737.4–022928A ^d	M Star	QORG				No
J043737.4–022928B ^d	Star	QORG				No
J052716.4+014840	Star	QORG				No
J073845.46+171249.1	Star	Optical	14.94	0.44	B	No
J074532.64+413633.8	Star	Optical	14.59	0.36	B	No
J075247.90+360110.4	Star	Optical	14.61	0.29	Both	Yes
J080520.22+064609.7	Star	Optical	14.92	0.26	B	No
J082507.20+200637.6	Star	Optical	14.99	0.23	B	Yes
J083121.17+475053.2	Star	Optical	14.06	0.32	B	Yes
J085825.29+073944.9	Star	Optical	14.48	0.52	A	Yes
J094141.91+572957.4	Star	Optical	14.52	0.47	A	Yes
J094949.12+031616.6	Star	Opt.+NIR	13.95	2.32		No
J095810.81+014218.7	Star	Optical	14.61	0.33	A	No
J100505.03+431735.9	Star	Optical	14.59	0.66	B	Yes
J102700.00+390804.2	Quasar	X-ray source	16.55 ^e	1.65		Yes
J103858.44+401058.4	Quasar	X-ray source	15.91 ^e	1.15		Yes
J104420.11+024819.8	Quasar	radio+NIR	16.28	2.00		No
J104505.17+084339.1	Quasar	Opt.+NIR	15.76	1.98		Yes
J105756.30+092314.9	CV ^f	Optical	14.94	0.23	A	Yes
J110533.55+335234.4	Star	Opt.+NIR	10.88	0.87		No
J111612.37+494211.6	Star	Opt.+NIR	10.91	0.81		No
J112632.90+120438.0	Quasar	X-ray source	20.39	1.04		Yes
J114913.1–0021136.1	Star	Optical	14.71	0.71	B	No
J121905.30+210633.5	Extended Source	X-ray source	14.83 ^e	1.16		No
J124127.66+085219.5	Quasar	radio+NIR	16.29	1.49		yes
J124320.01+010844.0	Star	Opt.+NIR	14.30	0.85		No
J131204.71+064107.6	Quasar	Opt.+NIR	16.00	1.94		Yes
J134517.99+280116.3	Star	Opt.+NIR	14.94	1.45		No
J135104.50+064307.1	Star	Opt.+NIR	15.94	1.63		No
J143008.65+230621.6	Seyfert	X-ray source	16.05 ^e	1.47		No
J143334.42–035626.7	Unknown	Opt.+NIR	12.03	0.85		No
J143505.34+404219.4	M Star ^g	Opt.+NIR	15.12	1.89		No
J145426.43+181951.8	Star	X-ray source ^h	12.77	1.14		No
J145434.35+080336.7	Quasar	Opt.+NIR	15.83 ^e	2.03		Yes
J150017.58+121036.5	Star	Opt.+NIR	15.99	0.99		Yes
J150859.72+265148.2	Star	Opt.+NIR	11.50	0.84		No
J151224.30–001830.4	Star	Opt.+NIR	15.69	1.71		No
J153334.69+051311.4	Seyfert	radio+NIR	15.89	1.34		Yes

Table 1—Continued

Name	Type ^a	Method	i^b	$J - K$	Group	SDSS? ^c
J153737.84+472604.0	M Star ^g	Opt.+NIR	15.43	2.85		No
J160731.42+173138.4	Seyfert	radio+NIR	16.53	1.38		No
J162808.20+634924.5	Quasar	X-ray source		1.67		
J164016.12+295336.3	Star	Optical	14.82	0.61		Yes
J164154.20+151753.5	Extended Source	X-ray source		1.58		
J170511.22+225128.4	Star	Opt.+NIR	15.77	1.01		No
J170707.96+222428.2	M Star ^g	Opt.+NIR	15.09	2.34		No
J172832.91+621622.4	M Star ^g	radio+NIR	17.10	1.51		No
J175740.20+565508.0	Quasar	X-ray source		1.70		
J184147.00+321838.5	Extended Source	X-ray source		1.41		

^aClassification is based on FWHM of $H\alpha$ line ($> 1000\text{km sec}^{-1}$ for quasar) and the i-band absolute magnitude ($M_i < -22.0$ for quasar; Schneider et al. 2003).

^bWe use PSF magnitude for point sources and Petrosian magnitude for extended sources.

^cAlso selected as a quasar candidate in SDSS?

^dThese two objects are different from each other. We could not identify which one is the target since they are located very close to each other.

^eExtended source. We use Petrosian magnitude for extended sources, while we use PSF magnitude for point sources.

^fCataclysmic variable

^gThe classification may represent that of a nearby bright star. See text.

^hA galaxy is located $12.06''$ from this object. It is possible that this galaxy is the X-ray source since the position accuracy of *ROSAT* is worse than $13''$.

Table 2. Observation summary

Date	Weather	Seeing('')	Cand.# ^a	Wavelength coverage
2005 Jan 5	clear	3.2	18	5,000 – 10,000Å
2005 Jan 6	humid	2.2	2	
2005 Jan 7	cloudy	4	6	
2005 May 9	partly cloudy	3.3	11	4,200 – 8,400Å
2005 May 10	cloudy	3.3	4	
2005 May 12	humid	2.8	1	
2005 May 13	cloudy	3.1	7	
2005 May 14	clear	2.5	10	
2006 Jun 17–24		2.5–3.5	3 ^b	4,200 – 8,400Å
2006 Dec 20–25		2.5–3.5	2 ^b	4,200 – 8,400Å

^aNumber of observed candidates

^bExcluded low-*b* objects that were the main targets of those observation runs.

Table 3. Properties of quasars

SNUQSO Name	z	$FWHM_{H\alpha}$ [km s ⁻¹]	$FWHM_{H\beta}$ [km s ⁻¹]	$Flux_{H\alpha}$ [$\times 10^{-15}$ erg s ⁻¹ cm ⁻²]	$Flux_{H\beta}$ [$\times 10^{-15}$ erg s ⁻¹ cm ⁻²]	M_{BH} [$\times 10^6 M_{\odot}$]	SDSS? ^a R^* ^b	M_g	M_i
J003236.59-091026.2	0.092 \pm 0.001	1856 \pm 307	2022 \pm 568	493 \pm 62	152 \pm 32	25.7 ^{+9.3} _{-8.7}	N	4.8	-22.75 -23.16
J102700.00+390804.2	0.144 \pm 0.001	2645 \pm 356	1651 \pm 678	104 \pm 13	12.5 \pm 4.6	33.1 ^{+11.6} _{-10.7}	Y	\searrow 3.1	-21.80 -22.37
J103858.44+401058.4	0.091 \pm 0.002	1267 \pm 1188		7.49 \pm 5.89		1.04 ^{+2.08} _{-2.07}	Y	\searrow 2.5	-20.99 -22.01
J104420.11+024819.8	0.101 \pm 0.001	1289 \pm 536	987 \pm 480	80.2 \pm 23.9	8.23 \pm 3.08	4.99 ^{+4.47} _{-4.42}	N	10.3	-21.23 -22.10
J104505.17+084339.1	0.123 \pm 0.001	3776 \pm 627	4854 \pm 2122	359 \pm 58	95.2 \pm 41.0	116 ⁺⁴⁷ ₋₄₅	Y	13.0	-22.00 -22.83
J112632.90+120438.0	0.977						Y	\searrow 1.1	-27.50 -27.65
J124127.66+085219.5	0.129 \pm 0.002	1470 \pm 470		31.1 \pm 8.9		5.16 ^{+3.64} _{-3.58}	N	2.2	-22.00 -22.65
J131204.71+064107.6	0.239 \pm 0.001	7402 \pm 608	8825 \pm 1924	677 \pm 55	124 \pm 27	1320 ⁺³⁶⁰ ₋₃₂₀	N	\searrow 1.5	-23.73 -24.02
J143008.65+230621.6	0.079 \pm 0.001	4674 \pm 1159	8506 \pm 2383	110 \pm 27	36.1 \pm 10.0	58.1 ^{+32.3} _{-32.0}	Y	\searrow 3.5	-20.29 -21.57
J145434.35+080336.7	0.131 \pm 0.001	2391 \pm 540	2574 \pm 613	393 \pm 84	46.7 \pm 10.6	50.6 ^{+26.3} _{-25.5}	N	10.9	-21.98 -22.78
J153334.69+051311.4	0.038 \pm 0.001	4446 \pm 531	5757 \pm 1699	169 \pm 25	20.6 \pm 6.0	31.6 ^{+10.4} _{-9.5}	N	2.5	-19.43 -20.24
J160731.42+173138.4	0.085 \pm 0.001	1459 \pm 315	716 \pm 670	59.5 \pm 7.3	7.02 \pm 6.83	4.48 ^{+2.20} _{-2.12}	N	5.8	-20.01 -21.44
J162808.20+634924.5	0.104 \pm 0.001	2103 \pm 420	1703 \pm 562	82.2 \pm 15.1	18.0 \pm 5.4	12.9 ^{+6.0} _{-5.8}	N	\searrow 2.0	-21.52 ^c
J175740.20+565508.0	0.174 \pm 0.001	2269 \pm 869	2769 \pm 2031	44.6 \pm 16.1	17.3 \pm 12.2	18.5 ^{+15.5} _{-15.3}	N	\searrow 4.9	-21.73 ^c

^aAlso discovered as a quasar by SDSS?, Y=Yes, N=No

^bRadio loudness

^c B -band magnitude (Vega)

Table 4. Efficiency for each method

Method	Observed	Discovered	Efficiency
Optical Multiple Color	17	1	5.9%
Optical+NIR	17	3	17.6%
Radio+NIR	5	4	80.0%
X-ray	10	6	60.0%
Qorg	6	0	0.0%

Table 5. Estimated properties of host galaxies

SNUQSO Name	σ [km s ⁻¹]	M_g [mag]	m_i [mag]	θ_{50} ^a [$''$]	Petro i –Fiber i ^b (measured),[mag]
J003236.59–091026.2	132	-19.1	17.7	1.3	
J102700.00+390804.2	141	-19.4	18.2	1.2	17.7
J103858.44+401058.4	60	-16.2	20.4	0.3	16.3
J104420.11+024819.8	88	-17.6	19.4	0.6	
J104505.17+084339.1	192	-20.5	16.7	2.7	
J112632.90+120438.0					
J124127.66+085219.5	89	-17.7	19.9	0.5	17.1
J131204.71+064107.6	353	-22.7	16.0	6.0	
J143008.65+230621.6	162	-21.5	16.4	2.8	16.5
J145434.35+080336.7	157	-19.7	17.7	1.7	17.2
J153334.69+051311.4	139	-19.3	15.5	3.9	16.9
J160731.42+173138.4	86	-17.5	19.1	0.6	17.3
J162808.20+634924.5	111	-20.1	18.4	1.0	
J175740.20+565508.0	122	-18.8	19.2	0.8	

^aHalf light radius

^bWe list only objects with visible hosts.